NREL
NATIONAL RENEWABLE ENERGY LABORATORY

Dynamic Model Validation of PV Inverters Under Short-Circuit Conditions

Preprint

E. Muljadi, M. Singh, and V. Gevorgian
National Renewable Energy Laboratory

R. Bravo
Southern California Edison

To be presented at the IEEE Green Technologies Conference
Denver, Colorado
April 4–5, 2013

Conference Paper
NREL/CP-5500-57341
March 2013

Contract No. DE-AC36-08GO28308

Available electronically at http://www.osti.gov/bridge

Available for a processing fee to U.S. Department of Energy
and its contractors, in paper, from:

U.S. Department of Energy
Office of Scientific and Technical Information
P.O. Box 62
Oak Ridge, TN 37831-0062
phone: 865.576.8401
fax: 865.576.5728
email: mailto:reports@adonis.osti.gov

Available for sale to the public, in paper, from:

U.S. Department of Commerce
National Technical Information Service
5285 Port Royal Road
Springfield, VA 22161
phone: 800.553.6847
fax: 703.605.6900
email: orders@ntis.fedworld.gov
online ordering: http://www.ntis.gov/help/ordermethods.aspx

Cover Photos: (left to right) PIX 16416, PIX 17423, PIX 16560, PIX 17613, PIX 17436, PIX 17721

Printed on paper containing at least 50% wastepaper, including 10% post consumer waste.

Dynamic Model Validation of PV Inverters Under Short-Circuit Conditions

E. Muljadi, *Fellow, IEEE,* M. Singh, *Member, IEEE*, R. Bravo, *Member, IEEE,* V. Gevorgian, *Member, IEEE*

***Abstract*—Photovoltaic (PV) modules have dramatically decreased in price in the past few years, spurring the expansion of PV deployment. Residential and commercial rooftop installations are connected to the distribution network; large-scale installation PV power plants have benefited from tax incentives and the low cost of PV modules.**

As the penetration of PV generation increases, the impact on power system reliability will also be greater. Utility power system planners must consider the role of PV generation in power systems more realistically by representing PV generation in dynamic stability analyses. Dynamic models of PV inverters have been developed in the positive sequence representation.

We developed a PV inverter dynamic model in PSCAD /EMTDC. This paper validates the dynamic model with an actual hardware bench test conducted by Southern California Edison's Distributed Energy Resources laboratory. All the fault combinations, symmetrical and unsymmetrical, were performed in the laboratory. We compared the simulation results with the bench test results.

***Index Terms*—photovoltaic, PV, dynamic model, validation, solar PV inverter, renewables**

I. Introduction

As shown by the graph in Figure 1, global photovoltaic (PV) installed capacity is growing exponentially. This growth has been fueled by many factors, including supportive policy, short development time, and the decline of the cost of PV panels in recent years.

Many PV installations are rooftop installations within the distribution power system network. These are mostly funded by private homeowners or businesses. Although distribution circuits have limitations on the amount of generation that can be installed, this type of installation offers an advantage in the diversity of solar irradiation (it has a lower impact on voltage and frequency fluctuations) and may lower the need for some transmission lines.

Other PV installations are MW-scale PV power plants (PVPPs) located in remote, inexpensive real estate within solar-rich resource regions. Transmission lines are necessary to transmit the bulk power generated by these PVPPs.

During 2011, the PV market saw unprecedented growth and wide deployment of this environmentally friendly source of power generation. On a global scale, approximately 30,000 MW of new PV were added during 2011, raising the total installed capacity to almost 70,000 MW. This number has risen above the optimistic forecast contained in reference [1], and it translates into investments of more than €50 billion in 2010, also above the report's forecast.

In this report, current-voltage relationships of a single solar cell were expanded to a PV module and finally an array. There are numerous models for solar cell operation [2–6]. The five-parameter model given by Desoto et al. [7] uses the current-voltage relationship for a single solar cell and only includes cells or modules in series. The dynamic model presented uses the PV characteristics presented in [8], and the equations are not repeated in this paper.

This paper is organized as follows: Section II presents the PV inverter configuration. Section III describes the PV inverter characteristics. Section IV describes the PV inverter dynamic model validation. Finally, the summary and conclusion are given in Section V.

Figure 1 - Evolution of global cumulative installed capacity 2000-2011 (MW)

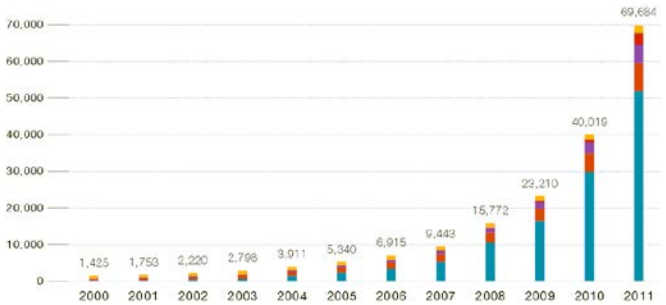

	2000	2001	2002	2003	2004	2005	2006	2007	2008	2009	2010	2011
ROW	751	807	887	964	993	1,003	1,108	1,150	1,226	1,306	1,209	1,717
MEA	N/A	N/A	N/A	N/A	N/A	N/A	N/A	N/A	N/A	21	205	336
China	19	30	45	55	64	68	80	100	145	373	893	3,093
America	146	177	222	287	379	498	645	856	1,205	1,744	2,820	5,053
APAC	355	491	677	902	1,178	1,475	1,797	2,080	2,643	3,409	5,116	7,769
Europe	154	248	389	590	1,297	2,299	3,285	5,257	10,554	16,357	29,777	51,716
Total	1,425	1,753	2,220	2,798	3,911	5,340	6,915	9,443	15,772	23,210	40,019	69,684

Fig. 1. Global PV installation.

II. PV Inverter Configuration

In a PVPP, the number of PV arrays connected to the power converter depends on the size of the PV inverters. Most PV inverters in the low power level (less than 10 kW) are usually configured as a single-phase inverter (up to 240 V for residential) or three-phase inverter (10 kW up to 15 kW for small, commercial installations connected at a line voltage of 208 V). A rating of 10 kW to 100 kW is considered small-medium commercial, and is usually configured using a three-phase inverter at a line voltage of 480 V. Three-phase inverters at 100 kW have either 208-V or 480-V ratings. The power output of these inverters is usually 208 V, which is transformed to a higher voltage internally or externally to the inverter. Various types of step-up transformers are being used in these applications:

- A 208-V to 480-V internal transformer followed by a 480-V to 12-KV or 480-V to 33-KV external transformer that is interconnected to the distribution system
- A 208-V to 12-KV or 208-V to 33-KV external transformer that is interconnected to the distribution system

A. PV Array Connections

PV modules are mounted on a structure frame. The PV module can be built as a fixed structure, or it can be directed to maximize sun exposure. A single-axis tracking system allows the direction of the PV panel to be adjusted based on the seasonal position of the sun during the months of year (north-south). A dual-axis tracker allows an additional degree of freedom to track the hourly direction of the sun throughout the day (east-west).

In practice, several modules are connected to a combiner box to form strings of modules to achieve the desired ratings. Thus, a solar PV module array is connected to a PV inverter to convert from DC to AC. Figure 2 shows an example of connections of PV modules within a PVPP. Consider a string of 10 PV modules connected to form 3 kW of PV array with a maximum peak power tracker (MPPT) to adjust the voltage at the PV array terminals such that it will maximize its output power. The PVPP consists of rows of PV arrays. In Figure 2, two strings of PV arrays per row are combined to obtain a 6-kW output per row. There are 25 rows connected together to obtain an output of 150 kW.

B. MPPT

The use of MPPT is intended to maximize energy capture for a given solar irradiance. There are many types of MPPT implemented to harvest the maximum solar power from a PV array. The PV array characteristics are similar to the

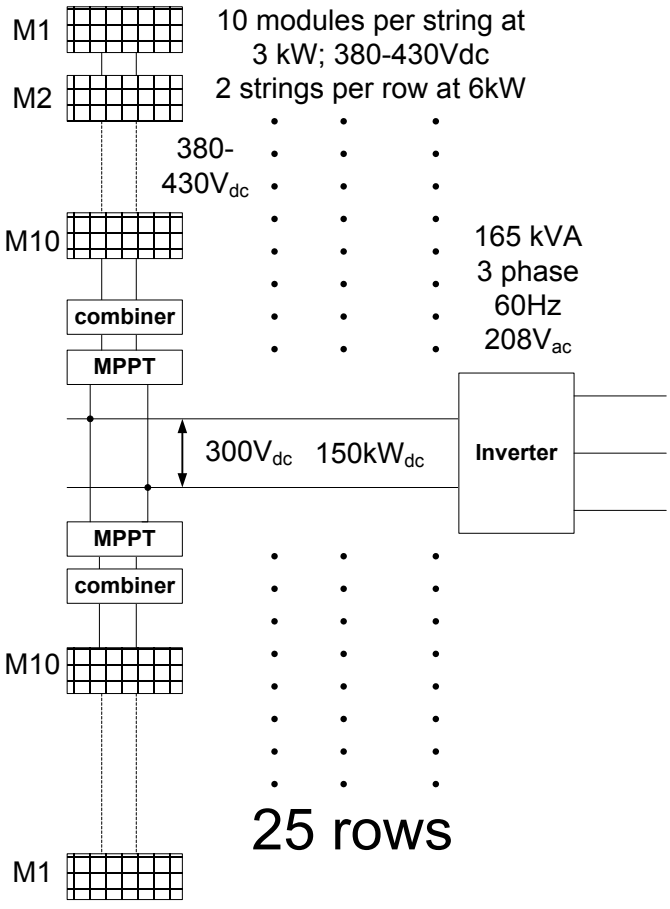

Fig. 2. The concept of a PV array connected to PV inverter.

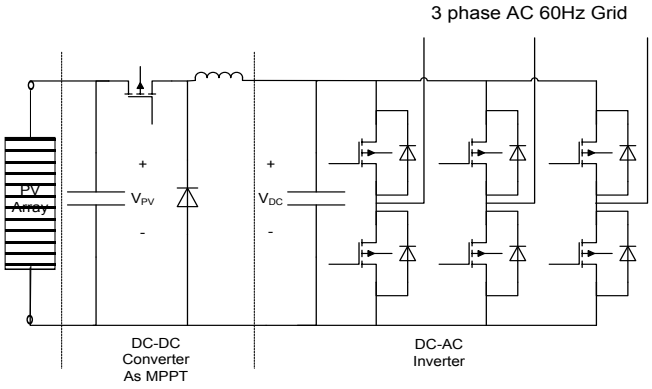

Fig. 3. A simplified PV system connected to the grid.

characteristics of a PV module; thus, they vary with solar irradiance and temperature. The idea behind MPPT is the same—i.e., the voltage of the array can be varied to maximize energy capture.

The MPPT can be implemented, internally or externally to the inverter, with many different types of DC-DC converters, or it may be implemented with a variable DC bus voltage. In most installations, the MPPT is located within the inverter. The MPPT controller can be implemented by a DC-DC converter connected to a constant-voltage DC bus. An example of MPPT implementation is shown in the simplified configuration in Figure 3. Among others, one type of DC-DC converter that can be utilized as an MPPT is a buck converter. The relationship between the V_{PV} and V_{DC} can be expressed by the following equation:

$$\frac{V_{PV}}{V_{DC}} = \frac{1}{D}$$

where D is the duty ratio of the DC-DC converter.

Many references can be found about the implementation of MPPT using different types of controllers; however, in this paper, we are more interested in the power system dynamics and do not focus on MPPT implementation.

C. PV Inverter

There is a special PV array configuration that has an MPPT at each of the solar PV arrays. Figure 2 shows ten modules connected to a combiner box. Each combiner box has its own MPPT, thus allowing the string of 10-PV modules to maximize its own power. The outputs of the MPPTs from all 25 rows of arrays are connected to the DC bus of an inverter rated at 165 kVA. The inverter rating is influenced by the overload capability and the power factor range required by the customer. Obviously, the more overload and the larger the power factor range required for this installation, the higher the rating of the inverter needed.

The PV inverter combines the output of rows of PV strings (see Figure 2) in DC and converted to AC. For this example, the inverter processes the output of PV arrays consisting of 500 PV modules. The three-phase output voltage of the inverter is at 208 V. A transformer is used to step up the voltage from 208 V to 480 V at 165 kVA. The rating of the power transformer is based on the assumption that the inverter

has to contribute reactive power to the grid. The size of the reactive power requirement depends on the request of the PVPP developer or the utility grid at the point of interconnection. The footprint of the PV array is large; thus, there is significant length of DC cables interconnected within the footprint of the PV array. To minimize the losses, the voltage of the collector system transmitting the output power to the substation transformer will be delivered at 34.5 kV. In Figure 4, a group of four transformers is shown connected to a three-phase step-up transformer rated at 480 V to 34.5 kV at 660 kVA.

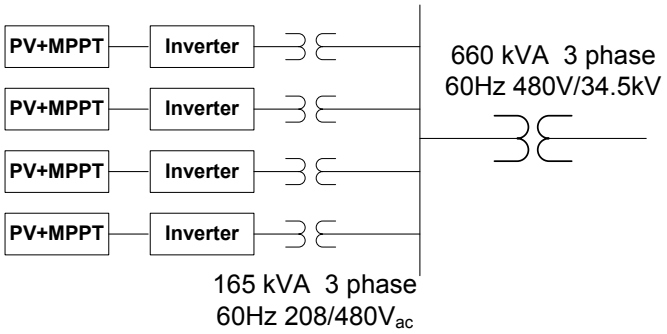

Fig. 4. Step-up transformer to deliver the output power at 34.5 kV to the substation transformer.

III. PV Inverter Characteristics

Historically, PV generation was developed on a very small scale based on small PV modules (50-W to 100-W ratings). For a long time, PV modules were very expensive and PV deployment was limited to isolated generation with battery storage. In early applications, the DC output was used to operate a radio, a light, or small tools. PV inverters were usually single-phase AC inverters at 60 Hz with output power less than 1 kW. Like any electrical appliance, small PV inverters are typically certified for safe application by Underwriters Laboratory (UL certification, UL 1741). The certification emphasizes the safe use of this equipment.

As the adaptation of PV generation gained momentum, small PV modules were connected on the rooftops of residential houses. The size still was very small and the cost of PV modules still was very high, thus the level of PV penetration was not considered to have any impact on the power system at the distribution network. If there were to be any grid disturbance, these small PV inverters would disconnect from the grid and then reconnect after some time when the disturbance had ended.

The size of PV modules and PV inverters increased while the cost continued to decrease. There were significant numbers of PV installations on the rooftops of commercial buildings. In many cases, the output power reached above a 100-kW rating. Circa 2003, IEEE issued a standard commonly known as IEEE 1547 to standardize the rules for connecting distributed generation (including PV inverters) to the distribution network. This standard was developed for low penetration of solar PV in the grid.

IEEE 1547 is intended to ensure that renewable energy generation does not violate some of the basic rules of the distribution system and ensure the safe and reliable operation of the distribution system. Conventional power flows from the generator into a residential load. With the increase of distributed generation such as PV generation, the power flow may reverse direction for the duration of a day when there is excess generation from the rooftop PV generating unit. Another concern is the safety of the utility service engineer performing repairs in the distribution network because of islanding when the PV generation keeps feeding the local load after the circuit breaker disconnects the load from the main distribution network.

PV inverter manufacturers strive to comply with IEEE 1547 [9–10], implement anti-islanding protection, and ensure that PV inverters stay connected within the allowable voltage-time and frequency-time operating region. Table 1 lists the operating voltage and the maximum clearing time for distributed generation. Table 2 lists the operating frequency and the maximum clearing time for distributed generation as specified in IEEE 1547 [11–12]. Figure 5 and Figure 6 are the graphical representations of Table 1 and Table 2, respectively.

Table 1. Voltage Range and Maximum Clearing Time

Voltage Range (% Nominal)	* Max. Clearing Time (seconds)
V < 50%	0.16
50% < V < 88%	2
V > 120%	0.16
110% < V < 120%	1

(*) Maximum clearing times for DER ≤ 30 kW; default clearing times for DER > 30 kW

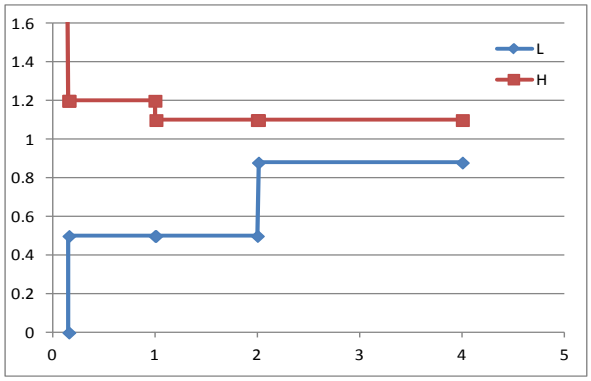

Fig. 5. Voltage versus maximum clearing time representation as described in the IEEE 1547.

Additional disconnection requirements include:

- Cease to energize for faults on the Area EPS circuit
- Cease to energize prior to circuit reclosure
- Detect island condition and cease to energize within 2 sec of the formation of an island ("anti-islanding")

Table 2. Frequency Range and Maximum Clearing Time

Frequency Range (Hz)	Max. Clearing Time (seconds)
f > 60.5	0.16
* f < 57.0	0.16
** 57.0 < f < 59.8	0.16 - 300

(*) 59.3 Hz if DER ≤ 30 kW
(**) For DER > 30 KW

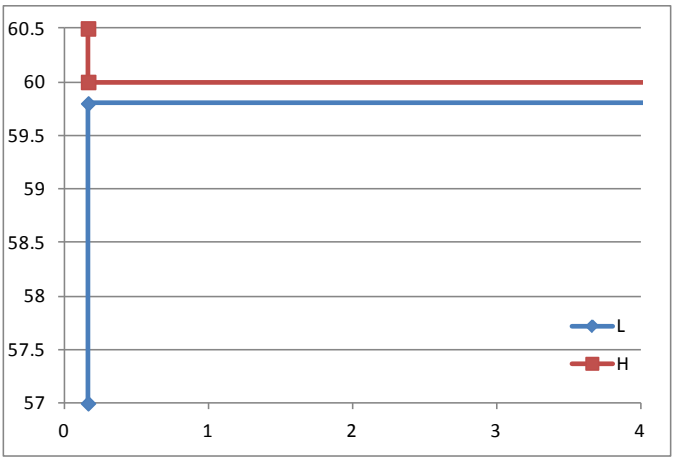

Fig. 6. Frequency versus maximum clearing time representation as described in IEEE 1547.

As the level of PV penetration continues to increase, fault ride-through capability, currently implemented for wind turbine generation, may be required for PV generation in the near future [13]. This requirement was placed to ensure that a wind plant would not be disconnected from the grid at any fault unless the voltage at the point of common coupling of the wind plant lies beyond the voltage-time characteristic specified; thus, balance between generation and load can be maintained, and the cascading phenomena can be avoided.

As described previously, the PV inverter is generally placed between the PV module or array and the grid; thus, the PV inverter must process the entire generated power to the grid. There are two types of protection in solar PV inverters: fast disconnection (i.e., in less than one cycle) and with continued operation for up to 10 cycles. The fast disconnection may be suitable for small PV installations connected to the grid or for isolated operations.

As summarized in [14], a PV inverter's current contribution during a fault is not zero and it varies by design. It was observed that, for most fault conditions, several PV inverters continued supplying current to the feeder subsequent to a fault for a period ranging from 4 to 10 cycles. The length of time the inverter supplies the fault current may be adjustable to comply with the regional reliability requirement. With reduced voltage, the output currents that can be supplied to the grid are limited by the current-carrying capability of the power electronics switches (i.e., IGBT); thus, the output power is less than the rated power. If low-voltage ride-through is available, during the voltage dip the MPPT may be disabled to ensure that the inverter follows the fault ride-through requirement rather than maximizing energy yield.

If the PV inverter is required to supply reactive power during the voltage dip, the PV inverter models may have to supply maximum reactive power available based on the current capability of the IGBT. The theoretical maximum reactive power contribution is when the voltage is leading or lagging 90 degrees. The PV inverter may be designed to carry short-term high current during the faults; many of them are designed to reach up to 120% or more of the rated current depending on the customer request.

In some inverter models, the inverter current during faults was maintained at the prefault inverter current with this current setting, and the transition back to normal operation does not affect the PV operation drastically.

Another mode of operation found in some inverter models is that the inverter current was dropped to zero and the inverter was disconnected in less than 0.5 cycles for a fault when the terminal voltage reached below 50% on any phase.

IV. PV Inverter Model Validation

The PV inverter model is developed on the PSCAD platform. The general module of a PV inverter model is kept the same, but the control parameters and the system protection are tuned to represent the power inverter being tested.

Two types of faults were performed: the single-line-to-ground and the three-phase-to-ground. The response of the power inverter was recorded and the simulation results were compared to the actual recorded data.

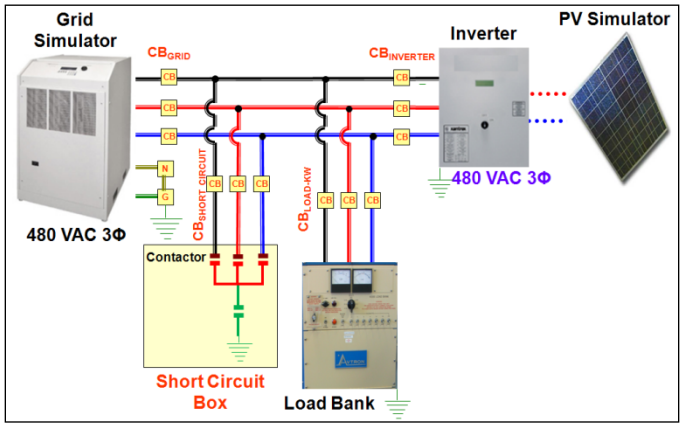

Fig. 7. Simplified diagram of bench test conducted by SCE.

A. Bench Test Diagram

The bench test conducted at Southern California Edison (SCE) is illustrated in the simple diagram presented in Figure 7. The grid simulator, load bank, short-circuit box, and solar PV were connected in parallel. The grid simulator was a programmable power supply that provided voltage reference for the inverter to start up. The PV simulator was a DC programmable power supply that allowed setting up the IV curve for the solar PV inverter input. The load bank was to consume the power and balance it to zero. The short-circuit box was used to apply the short circuits for any given combination—symmetrical or nonsymmetrical, ground faults

or nonground faults. The data was captured within a specified time window—prefault, during the fault, and post fault—to capture the transients and the action of the relay protection.

B. Unsymmetrical Fault—Single-Line-to-Ground

The single-line-to-ground (SLG) fault was performed for this power inverter by closing one of the phases (either A, B, or C) and the ground power contactors. The sequence equivalent circuit is presented in the Figure 8, with the sequence switches $S_{\_}$ and S_0 indicating the current controlled capability of the power inverter to generate only positive sequence currents, even during the faults. Note that the switches $S_{\_}$ and S_0 are not represented in a voltage source generator such as a conventional synchronous generator.

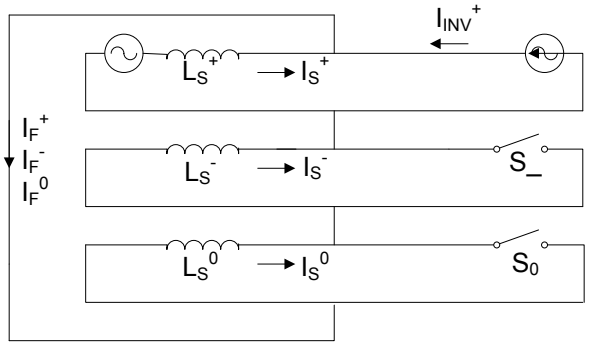

Fig. 8. The sequence equivalent circuit representing an SLG.

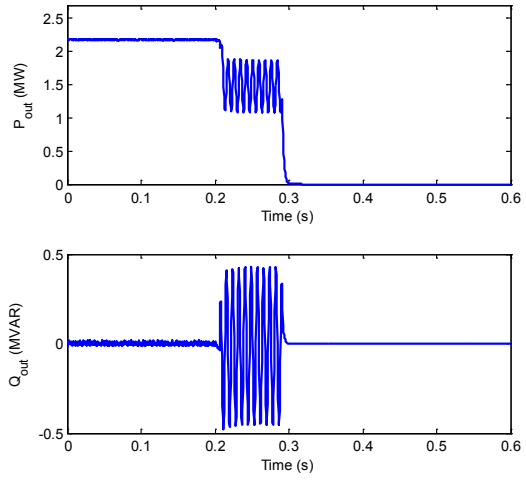

Fig. 9. The real and reactive power for a self-clearing SLG.

1) Phase current representation

A single-line-to-ground fault was simulated for this power inverter. The fault was a non-self-clearing fault occurring at *t=0.2s*. The power inverter was set to generate at a unity power factor, and the system was operating at 2.2 kW during normal operation (prefault).

As shown in Figure 9, the real power dropped by one-third of the prefault condition, then fell to zero as the inverter tripped offline. There were oscillations in the real and reactive power that were a result of phase imbalance, because the summation of the real and reactive power in the two active phases was not balanced. The reactive power stayed at zero before and after the fault.

2) Comparison Between Simulation and Lab Experimental Data for an SLG

In Figure 10, the comparison between the simulation and the measured data is shown on the same figure. The power inverter was set as follows:

- The output current was set at a unity power factor
- The short-term maximum output current was set at 100% rated current

The model relay protection was set to disconnect the power inverter after five cycles of low voltage (V < 50%) at any one of the phases.

It is shown that the simulation can follow the measured data very accurately, especially because the control system protection was set to follow the setting of the power inverter.

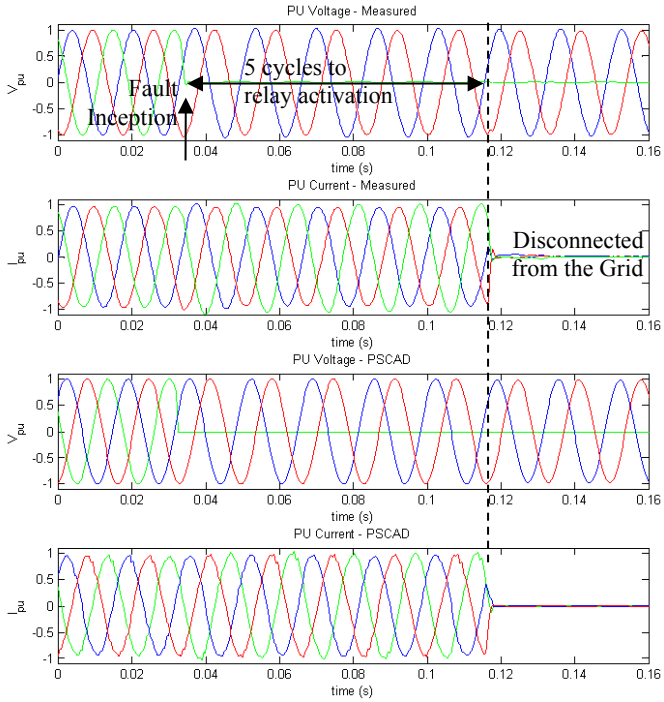

Fig. 10. Fault current contribution from a PV inverter for a single-line-to-ground fault.

3) Sequence Current Representation

Figure 11 shows the comparison of the sequence currents between the line contribution and the PV inverter contribution. The grid-side contribution of the fault current is shown in Figure 11 (a). The normal current in the prefault region was very small compared to the short-circuit current contribution from the grid during the fault. As shown in Figure 11 (a), the line contribution of the positive, negative, and zero sequence currents appeared on the grid contribution to the fault. All sequence currents (positive, negative, and zero) were equal in magnitude, as expected from an SLG.

In Figure 11 (b), the PV inverter contributed only positive sequence current, with a very small negative sequence (peak value at 0.1 p.u.) short-duration transient negative sequence current. Note that the PV inverter presented very large impedances to the negative and zero sequence currents (represented by the open switches $S_{\_}$ and S_0).

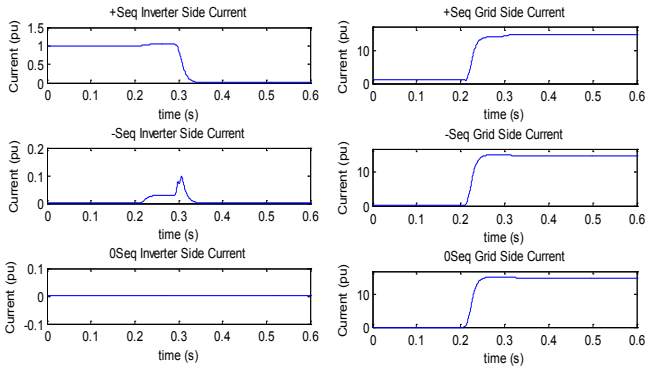

(a) Inverter-side sequence current contribution (b) Grid-side sequence current contribution

Fig. 11. The sequence current contribution from the PV inverter and the sequence current contribution from the grid for a single-line-to-ground fault.

C. Symmetrical Fault—Three-Phase Fault

Referring to Figure 7, the three-lines-to-ground (3LG) fault was performed for this power inverter by closing switches S_A, S_B, S_C, and S_G. The three phases were connected to the ground. Because this was a symmetrical fault, only the phase currents were presented. As expected, both the real power and reactive power dropped to zero as all three phases dropped to zero. In this case, as in the previous one, the fault was a non-self-clearing fault, at *t=0.2s*, and the inverter tripped offline because of the severity and duration of the fault.

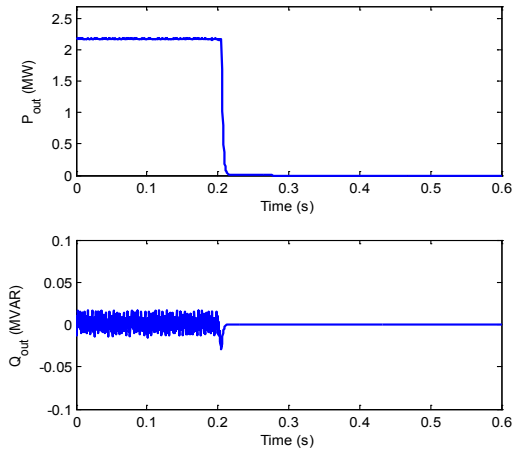

Fig. 12. The real and reactive power output of the PV inverter for a self-clearing 3LG.

1) Comparison Between Simulation and Experimental Data for a 3LG

Figure 13 shows the comparison between the simulation and the measured data. As shown, the simulation followed the measured data very accurately, especially because the control system protection was set to follow the setting of the power inverter.

The fault current in the three-phase output for this particular inverter was set to per-unit values.

For this particular inverter, the system protection was controlled to let the current flow to the fault for the duration of five cycles after the fault, and once one of the phases reached its zero crossing point, this particular phase was deactivated. The other two phases continued to supply output current until they reached the zero crossing point, then the last two phases were deactivated as well. Figure 14 shows the sequence currents; these behaved as expected for a balanced fault.

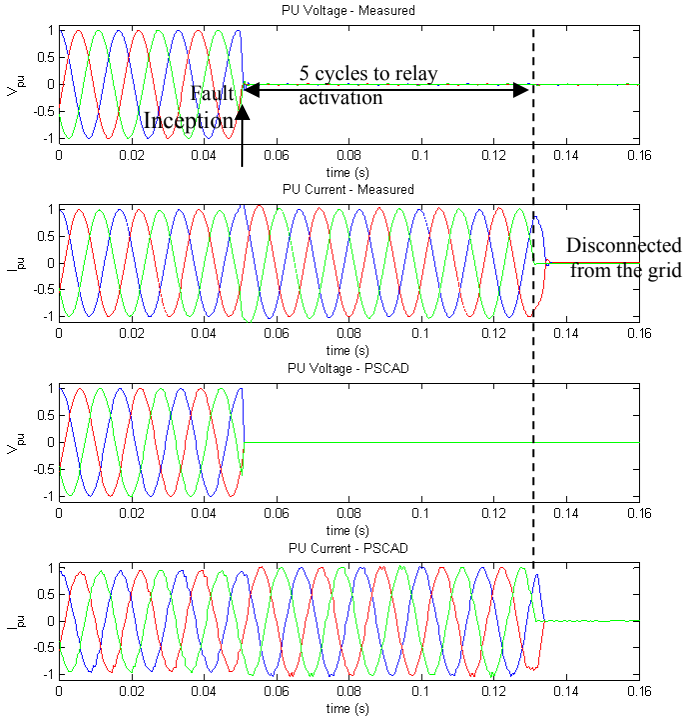

Fig. 13. The symmetrical 3LG was simulated on a PV inverter dynamic model and tested in the laboratory.

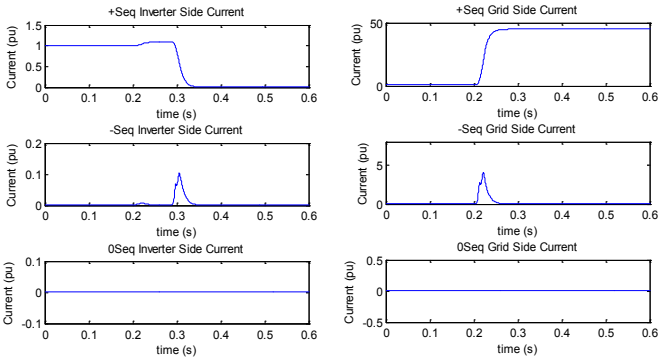

(a) Inverter side sequence current contribution (b) Grid side sequence current contribution

Fig. 14. The sequence current contribution from the PV inverter and the sequence current contribution from the grid for a three-phase-to-ground fault.

Figure 14 shows the sequence currents for the inverter-side contribution and the grid-side contribution. Because this was a 3LG, this fault was a symmetrical fault; thus, both the grid-side and the inverter-side short-circuit current contribution showed only the positive sequence components. The zero and negative sequence components appeared for only a short duration during the fault transient. We compared the results shown in Figure 14 to the results shown in Figure 11.

V. Conclusion

This paper was based on a collaboration between the National Renewable Energy Laboratory (NREL) and SCE. NREL developed the model for the PV inverter tested and validated in this paper. SCE provided the data for the validation of the dynamic model, which was developed on the PSCAD/EMTDC platform and created to model various PV inverters with many flexibilities in the implementation of different control algorithms for PV inverters.

Although the PV dynamic model presented in this paper was set to represent a specific power inverter tested at SCE, this model will be very useful to simulate other PV inverters developed by different manufacturers with different control modules inserted to represent manufacturer specific control algorithms and system protections.

VI. Acknowledgments

This work was supported by the U.S. Department of Energy under Contract No. DE-AC36-08-GO28308 with NREL. The tests were performed and funded by SCE.

VII. References

[1] E. Despotou, ed. "Global market outlook for photovoltaics until 2014," European Photovoltaic Industry Association, Brussels, 2010, www.epia.org/fileadmin/EPIA-docs/public/Global-Market-Outlook-for-Photovoltaics- until-2014.pdf.

[2] R. C. Campbell, "A circuit-based photovoltaic array model for power system studies," *39th North American Power Symp.*, pp. 97–101, 2007.

[3] D.S.H. Chan and J.C.H. Phang, "Analytical methods for the extraction of solar-cell single- and double-diode model parameters from i–v characteristics," *IEEE Trans. on Electron Devices*, vol. 34, pp. 286–293, 1987.

[4] R. Chenni, M. Makhlouf, T. Kerbache, and A. Bouzid, "A detailed modeling method for photovoltaic cells," *Energy*, vol. 32, pp. 1724–1730, 2007.

[5] M.W. Davis, B.P. Dougherty, and A.H. Fanney, "Prediction of building integrated photovoltaic cell temperatures," *J. of Solar Energy Eng.*, vol. 123, pp. 200–210, 2001.

[6] J.A. Duffie and W.A. Beckman, *Solar Eng. of Thermal Processes*. New Jersey: John Wiley & Sons, 2006.

[7] W. Desoto, S. Klein, and W. Beckman. "Improvement and validation of a model for photovoltaic array performance." *Solar Energy*, vol. 80, pp. 78–88, 2006.

[8] H. Tian, F. Mancilla-David, K. Ellis, E. Muljadi, and P. Jenkins, "A cell-to-module-to-array detailed model for photovoltaic panels," *J. of Intl. Solar Energy Society*, vol. 86, pp. 2695–2706, Sept. 2012.

[9] T. Basso, R. DeBlasio, "IEEE smart grid series of standards, IEEE 2030 (interoperability) and IEEE 1547 (interconnection) status," presented at Grid-Interop 2011, Phoenix, AZ, Dec. 5–8, 2011.

[10] "IEEE 1547, IEEE Standard for Interconnecting Distributed Resources with Electric Power Systems," *IEEE Standard Coordinating Committee 21*, Sponsored by Fuel Cell, Photovoltaic, Disperse Generation, and Energy Storage, 2003.

[11] A. Ellis, "IEEE 1547 and VRT/FRT for high penetration PV," presented at the UVIG Spring Technical Workshop, San Diego, CA, Apr. 12, 2012

[12] N. Miller, "IEEE Std 1547—Where are we going?" presented at the UVIG Spring Technical Workshop, San Diego, CA, Apr. 12, 2012

[13] C. Schauder, "Impact of FERC 661-A and IEEE 1547 on photovoltaic inverter design," presented at the IEEE Power and Energy Society General Meeting, Detroit, MI, July 24–29, 2011.

[14] W. Johnston and F. Katiraei, "Impact and sensitivity studies of PV inverters contribution to faults based on generic PV inverter models," *Ontario Grid Connection Study*, May 2, 2012.

VIII. Biographies

Eduard Muljadi (M'82, SM'94, F'10) received his Ph.D. in electrical engineering from the University of Wisconsin at Madison. From 1988 to 1992, he taught at California State University at Fresno. In June 1992, he joined NREL. His current research interests are in the fields of electric machines, power electronics, and power systems in general with an emphasis on renewable energy applications. He is member of Eta Kappa Nu and Sigma Xi, a Fellow of the Institute of Electrical and Electronics Engineers (IEEE), and an editor of the IEEE Transactions on Energy Conversion. He is involved in the activities of the IEEE Industry Application Society (IAS), Power Electronics Society, and Power and Energy Society (PES). He is currently a member of various committees of the IAS, and a member of the Working Group on Renewable Technologies and the Task Force on Dynamic Performance of Wind Power Generation, both of the PES. He holds two patents in power conversion for renewable energy.

Mohit Singh (M'11) received his M.S. and Ph.D. in electrical engineering from the University of Texas at Austin in 2007 and 2011, respectively. His research is focused on dynamic modeling of wind turbine generators. Dr. Singh is currently working at NREL as a postdoctoral researcher in transmission and grid integration of renewable energy. His current interests include modeling and testing various applications of wind turbine generators and other renewable energy resources. He is a member of the IEEE. He is involved in the activities of the IEEE Power and Energy Society.

Richard J. Bravo (M'2001) is a senior engineer in grid advancement at SCE. He has worked on various projects, including the upgrade of motor control centers for oil exploration, control system upgrades for pipelines and truck loading racks, SCE satellite communications, SCE's Delayed Voltage Recovery project, load performance during transient conditions, and SCE solar photovoltaic inverter generation performance in a distribution system. Bravo graduated from California State University at Long Beach with both a B.S. and an M.S. in electrical engineering. He earned a Power Systems Sequential Program Certificate from the University of California at Los Angeles and holds a Professional Engineer license in electrical engineering from the State of California.

Vahan Gevorgian (M'97) graduated from the Yerevan Polytechnic Institute in Armenia in 1986. During his studies, he concentrated on electrical machines. His thesis research dealt with doubly fed induction generators for stand-alone power systems. He obtained his Ph.D. in electrical engineering from the State Engineering University of Armenia in 1993. His dissertation was devoted to modeling electrical transients in large wind turbine generators. Dr. Gevorgian is a research engineer at the National Wind Technology Center of NREL. His current research interests include modeling and testing various applications of small wind turbine–based power systems.